



# Effect of high temperatures on the mechanical and thermal properties of Notre-Dame de Paris Lutetian limestone

Colin Guenser · Stéphane Corn ·  
Marie Salgues · Pierre Morenon ·  
Nathalie Domede

Received: 26 July 2023 / Accepted: 9 April 2024 / Published online: 29 April 2024  
© The Author(s), under exclusive licence to RILEM 2024

**Abstract** This study aims to determine mechanical and thermal properties of Saint-Maximin limestone, similar to the Lutetian stone found in the vaults of the Notre-Dame de Paris cathedral, and their variations after heating–cooling cycles at temperatures up to 800 °C. An extensive experimental campaign, including both destructive and non-destructive testing, was carried out. The results indicate that the samples can be considered to be isotropic, and the effect of temperature on Poisson’s ratio, static modulus of elasticity, compressive and tensile strengths were measured. Non-destructive testing revealed that the usual correlation equations between ultrasonic measurements and mechanical properties are not valid for heated stone samples, particularly when estimating Poisson’s ratio. An alternative measurement method using impulse modal analysis was proposed to overcome this issue. Uniaxial compressive tests on specimens of different geometries were used for the estimation of

shape factors specific to Saint-Maximin stone. Some of these shape factors contradict the current European standard for stone, which seems to overestimate the effect of slenderness. The study also suggests shape factors after heating at 300 °C and 600 °C to account for the effect of heating on the compressive strength. The results demonstrate that, while the correlations established for stones at room temperature remain valid, they are not necessarily accurate after a heating–cooling cycle. This study provides important information for the numerical modelling of this material from mechanical and thermal perspectives.

**Keywords** Limestone · High temperature · Destructive testing · Non-destructive testing · Mechanical behaviour · Thermal behaviour

## 1 Introduction

In France, as elsewhere in Europe, the pre-industrial built heritage is most often made up of stones bound together with mortar. The importance of these structures for society, as cultural sites, as places of worship, or to bear witness to historical events, leads us to question our capacity to restore masonry structures after a fire while preserving their authenticity. The burning of Notre-Dame de Paris (NDP) cathedral in 2019 makes this question particularly topical. This long fire (15 h between its outbreak and its extinction), in which flame temperatures probably reached

---

C. Guenser (✉) · P. Morenon · N. Domede  
LMDC, Université de Toulouse, INSA/UPS Génie Civil,  
135 Avenue de Rangueil, 31077 Toulouse Cedex 04,  
France  
e-mail: guenser@insa-toulouse.fr

C. Guenser · S. Corn · M. Salgues  
LMGC, IMT Mines Ales, Univ Montpellier, CNRS, Ales,  
France

P. Morenon  
Toulouse Tech Transfer, 118 Route de Narbonne, CS  
24246, 31432 Toulouse Cedex 04, France



1200 °C [1], had a deep impact on the masonry, including the side walls and the north, south and west gables. The thirteenth century cathedral's roof was damaged and the timber structure was completely destroyed. The vaults were especially affected, as they accumulated burning materials and molten lead spill on their extrados. On the other hand, their intrados remained exposed to a quasi-normal temperature, creating a strong thermal gradient through a thickness of only 15 cm to 25 cm, depending on the vault considered. The reduction in material properties such as strength and rigidity is the first concern when considering the rehabilitation of such structures. However, it should be noted that traditional masonry structures are often in a state of compressive stress far below their strength. Nevertheless, the change in material rigidity inevitably alters the balance of the structure to some extent and should not be overlooked. Other issues are also of great interest in the assessment of structural equilibrium, such as thermal shock when water is used to extinguish the fire. The change in water sorption characteristics due to high temperature, in addition to the water absorbed during fire extinguishing, can also lead to long-term pathologies of the limestone [2].

The aim of the present study is to determine the mechanical and thermal characteristics of a Lutetian limestone representative of that used in the vaults of NDP cathedral. These samples were subjected to temperatures ranging from 20 °C to 800 °C and then cooled. The evolution of the residual mechanical and thermal properties was studied according to the maximal temperature reached. These experimental results were obtained in order to feed dedicated 3D numerical models, in the framework of the DEMMEFI research project concerning the post-fire structural analysis of NDP cathedral.

Previous works have already studied the effect of high temperatures on various types of stones and, above all, shown the great variability of the results depending on the stone considered, even within a lithology as specific as that of limestone [3]. There are widely acknowledged correlation equations from the theory of the propagation of elastic waves that enable mechanical parameters to be estimated from ultrasound (US) measurements, and numerous correlation equations between certain mechanical and physical parameters of limestones have been proposed [4]. However, these studies also reveal a great variability

depending on the type of stone, even among limestones alone. The relationship between dynamic and static measurements of modulus of elasticity is complex and require additional parameters such as density, porosity and compressive strength [5]. Furthermore, there is no information regarding correlation equations on heated stone. Some mechanical and thermal characteristics of 'franche fine' Saint-Maximin stone, typical of the stone encountered in NDP cathedral, exist in the literature for room temperature and high temperature [6, 7], but are not sufficient to feed the calculation code developed in the framework of the project and do not give any information regarding a possible anisotropy of the material.

The properties needed concern the stone's linear and non-linear mechanical characteristics (modulus of elasticity, Poisson's ratio, compressive and tensile strengths, peak compression strain value, and dilatancy) and thermal characteristics (thermal conductivity, heat capacity, and density). Values of these parameters before heating and after one heating/cooling cycle are needed to consider both unaltered material and post-fire residual material. In addition, the effect of size and shape should not be overlooked when undertaking rock strength tests [8]. By performing compression tests on specimens of different sizes, it will be possible to discuss compressive shape factors provided by the standard EN 772-1, as those provided by the Standard are applicable to a wide range of masonry units. Shape factor will also be discussed for heated and cooled stones.

Prior to the experimental campaign, the first step was to explore, as widely as possible, all the temperatures that the NDP cathedral stones could have been exposed to during the fire. Some samples were subjected to ambient temperature (20 °C), then to one temperature between 200 °C and 800 °C in steps of 100 °C. The specimens were heated, cooled, and finally tested by non-destructive methods. This first step allowed the overall post-fire behaviour of the samples to be apprehended for any temperature reached. Particular attention was also paid to estimating the anisotropy of the stone.

In a second phase, the main experimental campaign was performed. Extensive tests were carried out on unaltered samples and on samples subjected to two different heating/cooling scenarios only, in order to reduce the number of samples needed. These two scenarios were selected among those used in the



first phase so as to accurately depict the evolution of the material degradation with temperature. A significant number of specimens of different geometries was dedicated to each of the scenarios. The in-depth experimental campaign included non-destructive and destructive mechanical tests, so as to establish a connection between the laboratory characterization and previous in-situ measurements. Thermal characterization tests were also carried out.

## 2 Materials and methods

### 2.1 Materials

The choice of stone was based on a search for the greatest similarity with the materials identified in the vaults of the NDP cathedral. Among the different limestone studied on the site [9], the Saint-Maximin stone was identified in the areas rebuilt during the nineteenth century restoration campaign supervised by Viollet-le-Duc. This stone was chosen for this reason, and obtained from a quarry close to Paris (Oise, France). Among the Saint-Maximin stones, the “Ferme Fine” bed was selected for the similarity of its characteristics with those determined by the Laboratoire de Recherche des Monuments Historiques (LRMH) on the stones from the collapsed vaults of NDP cathedral [9].

Saint-Maximin “Ferme Fine” stone is commonly used as a building/restoration material for historical monuments. It is very similar in appearance to the Saint-Maximin “Franche Fine” studied by Vigroux (7), although the different name indicates a difference in aesthetics, mechanical quality, or both. It has

a beige colour and fine grain. Saint-Maximin stone is a Lutetian limestone from the Eocene, with scarce presence of fossils. It is a sedimentary limestone with barely visible bedding planes, which are represented by ‘=’ in Fig. 1.

To suit the different tests planned, the material was supplied in prisms, cubes and cylindrical cores, the last being extracted from blocks with initial dimensions  $l \times L \times h = 35 \times 35 \times 14$  (cm). This allowed the effects of slenderness and volume to be studied with the different test methods used. The thermal tests required powder samples and small disk samples 2.5 cm in diameter, extracted from the same samples after the mechanical tests had been completed. The samples were stored indoors and were considered to be dry (mass variation of less than 0.1% after 24 h at 70 °C).

The density measurements gave an idea of the dispersion present in the batch of samples used for this study: the average was 1757 kg/m<sup>3</sup>, with a coefficient of variation (CV) of 1.7% over 72 specimens. The absolute densities measured with a pycnometer at 20 °C gave an average value of 2738 kg/m<sup>3</sup> with a CV of 0.3% on nine randomly chosen powder samples. The stones are very porous, with an absolute porosity of 36%.

### 2.2 Heating and cooling protocol

The process of heating and cooling the specimens was a key element of this study. The thermal degradations studied here were those due to the increase in temperature in the material and not those due to differential thermal expansion. The computation code is precisely designed to calculate this type of structural

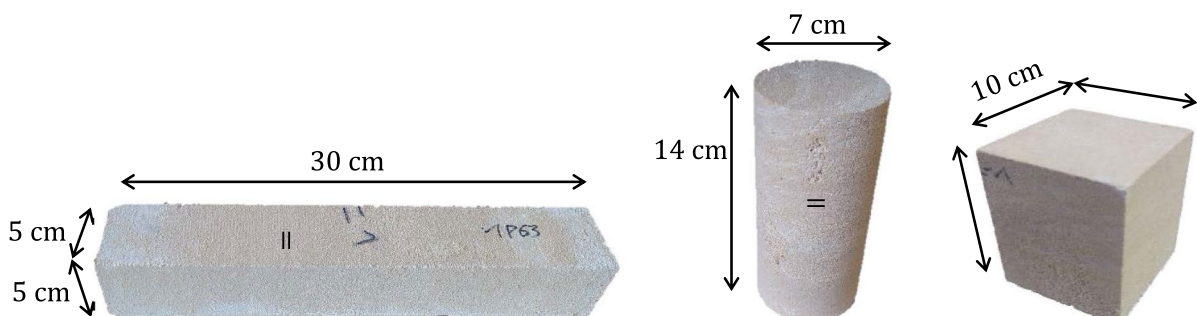


**Fig. 1** Sizes used for the mechanical tests

degradation, so the heating process had to ensure that samples were heated to a uniformly distributed temperature, and that the thermal gradient was kept to a minimum.

To ensure that the above criteria were respected, the heating protocol chosen was to heat the specimens to the target temperature at a rate of 5 °C/min and to allow a 5 h hold period at the target temperature. The specimens were allowed to cool with the oven switched off, which gave a cooling rate slower than 5 °C/min. This heating–cooling cycle was performed with an Enitherm DP46 electric furnace. The standard fire curve from ISO 834 [10] was not suitable as a heating protocol since it would inevitably have induced unwanted thermal stresses within the samples.

### 2.3 Testing protocols

The properties studied here were measured using several methods in order to be able to compare the results obtained. More specifically, mechanical elastic properties were first obtained by measurement of the velocity of US and also by Impulse Modal Analysis. Then, quasi-static compressive tests were performed to measure mechanical elastic properties and failure properties, i.e. compressive strength and

peak compressive strain. Three-point bending (3PB) tests were finally performed to obtain tensile failure properties.

The parameters measured in this study are presented in Table 1.

#### 2.3.1 Ultrasonic measurements

Non-destructive ultrasonic methods are commonly used on masonry stones, in particular to diagnose damage to structures [11]. In order to characterize the material and to link the results with non-destructive measurements performed at NDP [12], non-destructive ultrasonic (US) testing was performed on the samples according to EN 14579 [13]. This consisted of measuring the velocity of the primary waves,  $V_p$ , and secondary waves,  $V_s$ , using Pundit PL-200 equipment. The modulus of elasticity,  $E_{US}$ , and the Poisson's ratio  $\nu_{US}$  were derived from  $V_p$  and  $V_s$  using Eqs. 1 and 2 from the theory of propagation of elastic waves [14]. This protocol was applied to 5 cm × 5 cm × 30 cm prisms, 7 cm × 14 cm cylinders, and 35 cm × 35 cm × 14 cm blocks. It should be noted that  $V_s$  measurements are best performed on samples with lateral dimensions greater than their thickness [15], and that prisms and cylinders do not satisfy this condition. It is therefore not possible to

**Table 1** notations of the parameters measured

$E_{stat}$	Static modulus of elasticity on 7 cm × 14 cm cylinders
$E_{US}$	Dynamic modulus of elasticity by UltraSonic testing
$E_{IMA}$	Dynamic modulus of elasticity by Impulse Modal Analysis
$\nu_{stat}$	Static Poisson's ratio
$\nu_{US}$	Dynamic Poisson's ratio by UltraSonic testing
$\nu_{AMI}$	Dynamic Poisson's ratio by Impulse Modal Analysis
$\sigma_{c,10}$	Compressive strength on 10 cm × 10 cm × 10 cm cubes
$\sigma_{c,5}$	Compressive strength on 5 × 5 × 5 cm cubes
$\sigma_{c,7}$	Compressive strength on 7 cm × 14 cm cylinders
$\sigma_t$	Tensile strength obtained indirectly by three point bending test
$V_p$	Ultrasonic P-wave velocity
$V_s$	Ultrasonic S-wave velocity
$\epsilon_{c,peak}$	Strain at compressive stress peak
$\lambda_c$	Thermal conductivity on cooled materials (from hot wire testing)
$\lambda_h$	Thermal conductivity on hot materials (from XFA/DSC testing)
$c_{p,DSC}$	Heat capacity on hot materials (from DSC testing)
$C_{p,calo}$	Heat capacity on hot materials (from calorimeter testing)
$\alpha_h$	Thermal diffusivity on hot materials
$\rho$	Specific weight



accurately measure  $V_s$  on heated samples, since the  $35 \times 35 \times 14$  cm<sup>3</sup> blocks do not fit in the furnace. Furthermore, and according to the equipment manufacturer, the minimum sample width for  $V_p$  measurements should be equal to the wave length of P-waves and is estimated at 5.3 cm for the Saint-Maximin stone.

$$E_{us} = \rho \frac{V_p^2(1 + \nu)(1 - 2\nu)}{1 - \nu} \quad (1)$$

$$\nu_{us} = \frac{\frac{1}{2} - \left(\frac{V_s}{V_p}\right)^2}{1 - \left(\frac{V_s}{V_p}\right)^2} \quad (2)$$

Indices of the anisotropy of the stone can be estimated using Eqs. 3 and 4 from [16], estimated to be best suited for determining the anisotropy of rocks [17].

$$dM\% = \left[ 1 - \left( 2 \times \frac{V_{p,\min}}{V_{p,\text{mean}} + V_{p,\max}} \right) \right] \times 100 \quad (3)$$

$$dm\% = \left[ 2 \times \frac{V_{p,\max} - V_{p,\text{mean}}}{V_{p,\text{mean}} + V_{p,\max}} \right] \times 100 \quad (4)$$

where  $V_{p,\min}$ ,  $V_{p,\max}$ , and  $V_{p,\text{mean}}$  are the minimum, maximum and intermediate velocities of the three velocities measured in the orthogonal directions.

### 2.3.2 Impulse modal analysis

A non-destructive measurement method by Impulse Modal Analysis (IMA) is implemented in order to measure the elastic properties of the samples (modulus of elasticity  $E_{\text{IMA}}$ , Poisson's ratio  $\nu_{\text{IMA}}$ ) [18]. This method has the advantage of being based on the vibrational frequency of the sample instead of on a pulse travel time, and is therefore considered to give a better account of the evolution of the damage of the sample [19]. This method has already been used to monitor the damage caused to limestone by freeze–thaw cycles [20]. Considering the limits of the US stated above, the IMA allowed results to be obtained that could not be found rigorously with US. It is based on measuring the free vibration frequencies of the sample using an accelerometer. The resonance frequencies of bending and torsion modes

were measured after the sample was impacted with a ball in free fall. The frequency response spectrum was obtained and the Frequency Response Function (FRF) was calculated using the ModalView® software. The samples were placed on foam to model free suspension conditions. The resonance frequencies of the bending mode,  $F_f$ , and the torsion mode,  $F_t$ , were used to estimate  $E_{\text{IMA}}$  and  $\nu_{\text{IMA}}$ .

Considering the material to be relatively homogeneous (realistic assumption in the case of Saint-Maximin stone) and isotropic (hypothesis to be checked), the elastic mechanical properties of the samples were determined using the analytical expressions 5 and 6. These expressions link  $F_f$  and  $F_t$  to the desired mechanical properties. The values of the shape coefficients  $C_f$  and  $C_t$  were obtained via a preliminary numerical modal analysis of the sample with the Comsol Multiphysics® finite element software. These coefficients were calculated for different values of  $\nu$  in the interval [0; 0.5], and do not depend on  $E$ . The shape coefficients calculated for such prisms are described by Eqs. 7 and 8. As predicted by Eqs. 5 and 6,  $C_f$  (unlike  $C_t$ ) depends on the Poisson's ratio. In this study,  $C_t$  was taken to be 2.347 and  $C_f$  was taken to be 0.267, which corresponds to a  $\nu$  value of 0.25. The error on  $C_f$  is less than 2% for  $\nu$  ranging from 0.1 to 0.4. A similar analysis, performed for the 7 cm  $\times$  14 cm cylindrical samples, led  $C_t$  to be taken equal to 12.719 and  $C_f$  equal to 4.689.

$$F_f^2 = C_f(\nu, h, L) \times \frac{E_{\text{IMA}}}{\rho} \quad (5)$$

$$F_t^2 = C_t(b, h, L) \times \frac{G_{\text{IMA}}}{\rho} \quad (6)$$

$$\text{where } G_{\text{IMA}} = \frac{E_{\text{IMA}}}{2(1 + \nu_{\text{IMA}})}$$

$$C_f = 0.270 - 0.011 \times \nu \quad (7)$$

$$C_t = 2.347 \quad (8)$$

### 2.3.3 Quasi-static tests

The mechanical characteristics were determined by uniaxial compression and 3PB under quasi-static conditions according to the standards EN 12372 and EN 772–1 [21, 22].



The cylinders were used for uniaxial compression tests on a Criterion 45 MTS hydraulic press. To maximize the chance of measuring a post-peak softening, the test was done with a displacement rate set at 1 mm/min until failure. The lower plate of the apparatus was hinged. Each cylinder was instrumented with two longitudinal and two transversal gauges placed in the middle third of the sample, by means of which the strain at the compressive peak  $\epsilon_{c,peak}$ , the static modulus  $E_{stat}$  and the static Poisson coefficient  $\nu_{stat}$  were calculated. The value of the maximum force was recorded in order to estimate the compressive strength,  $\sigma_{c,7}$ .

The 10 cm × 10 cm × 10 cm cubes were used for uniaxial compression tests, with the load rate set at 0.15 MPa/s until failure according to EN 772–1 [22]. The compressive strength,  $\sigma_{c,10}$ , was recorded.

The prisms were used for 3PB. The distance between the supporting rollers was 250 mm and the rollers were 60 mm in diameter. The displacement at mid-span of the sample was set at a rate of 0.1 mm/min. The value of the maximum force,  $F_t$ , was recorded so that the tensile strength,  $\sigma_t$ , could be derived from Eq. 9 of the standard. To allow post-peak softening to appear, the samples were notched on the underside at mid-span, 8 mm deep and 2.7 mm wide.

$$\sigma_t = \frac{3F_t L}{2bh^2} \quad (9)$$

The undamaged ends resulting from the 3PB, equivalent to 5 cm × 5 cm × 5 cm cubes, were then used for compression tests carried out on a 3R Rp 400 hydraulic press. The test was run at a load rate of 0.25 MPa/s until failure and the compressive strength  $\sigma_{c,5}$  was recorded.

### 2.3.4 Thermal tests

The thermal conductivity of the samples was determined using transient methods. The first one was the hot wire measurement method, a method from which the hot disk method is derived [23]. The two ends resulting from the 3PB tests were used to perform conductivity measurements with a Neotim FP2C conductivity meter. This method consists of placing a heating wire and a thermocouple between two samples of materials. The wire heats the materials, and

the thermocouple records the rate at which the heat is absorbed by the material. The power of the heat source was 0.7 W and the measurement time was set between 90 and 120 s. A calibrated weight of 1 kg was placed on top of the sample. The measurement obtained was a conductivity,  $\lambda_c$ , in W/m<sup>2</sup> K. This method has the advantage of being a direct measurement of conductivity, but it can only be performed on cooled materials.

A second thermal measurement method was set up to measure the thermal conductivity of the hot material, using Xenon Flash Analysis (XFA) and a Differential Scanning Calorimeter (DSC) to measure the thermal diffusivity,  $a$ , and heat capacity,  $C_p$  [24]. The conductivity was then derived using formula (11) below. The XFA 600 Linseis machine performed diffusivity measurements on material samples in the form of thin disks about 25 mm in diameter and 2 mm thick. The lower part of the sample was irradiated with a pulse of a given amount of energy. This resulted in a homogeneous temperature rise within the sample, which was measured with a high-speed infrared detector. From the curve of time vs. temperature rise, the embedded software calculated the thermal diffusivity,  $a$ . The XFA machine was able to heat the sample and measure diffusivity up to 480 °C. Three stone samples were selected at random, and two disks were extracted from each of them. Each disk was subjected to temperatures of 20 °C, 300 °C and, finally, 480 °C, and at least five measurements were performed at each temperature. In total, 41 measurements were made at 20 °C, 30 at 300 °C, and 32 at 480 °C.

A Perkin Elmer DSC 8500 provided the heat capacity,  $C_p$ , of the material. The DSC was able to heat the sample and allowed measurements of  $C_p$  up to 500 °C. Three stone samples were selected at random, and five powder samples of about 30 mg were taken from each. Each powder sample was subjected to temperatures of 20 °C, 300 °C and 500 °C, and one measurement was performed at each temperature. In total, 15 measurements were performed at each temperature.

Finally, heat capacity measurements were carried out on hot materials using a Calvet C80 calorimeter, which works on the same principle as the DSC but does not require the material to be ground to powder. The original microstructure of the sample was kept, and thermal properties were not altered. This



instrument can heat the sample up to 250 °C during the measurement.

The evolution of specific weight with temperature was deduced from [6], which gives valuable information about thermal dilatancy and weight loss of hot Saint-Maximin stone. The specific weights,  $\rho$ , obtained at 20 °C, 300 °C and 600 °C were respectively 1756 kg/m<sup>3</sup>, 1739 kg/m<sup>3</sup>, and 1686 kg/m<sup>3</sup>. The hot thermal conductivity of the material was then deduced using Eq. 10.

$$\lambda_h = a \times c_p \times \rho \quad (10)$$

### 3 Preliminary tests ranging from 20 °C to 800 °C

The first results presented for the preliminary tests concern the estimation of the anisotropy of the stone to verify the hypothesis made regarding the IMA testing method.  $C_p$  measurements were carried out on 12 blocks of dimensions 35 cm × 35 cm × 14 cm, with four measurements in each of the three directions. The density of these blocks was 1749 kg/m<sup>3</sup> on average, with a CV of 1%. In the directions of the sedimentation plane, the average  $V_p$  measurements were 2804 and 2799 m/s, while, in the perpendicular direction, the average was 2856 m/s, i.e. relative differences of less than 2%. The standard deviation of the measurements varied from 80 m/s to 157 m/s, or about 3% to 5% deviation from the mean value. The  $V_p$  measurements showed that the anisotropy of

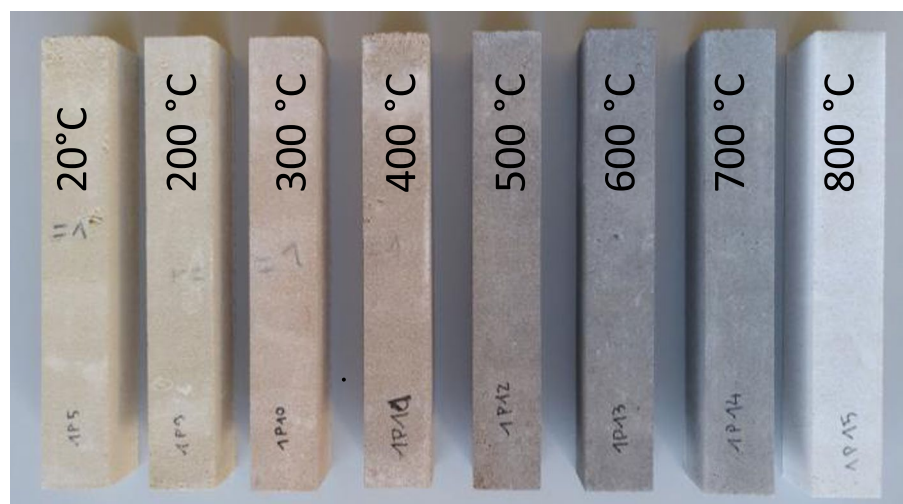
the stones was lower than the variability of the test method, which allowed the stones in the study to be considered as isotropic. Calculating the anisotropy indices from (3) and (4) yielded  $dM = 1.1\%$  and  $dm = 1.8\%$ , confirming the very low anisotropy of this stone, as already observed in [6]. Moreover, the velocity  $V_p$  (2842 m/s ± 4%) was in accordance with the range determined by Vigroux [6].

The  $V_s$  measurements were dependent on the length to width ratio of the geometry. It was therefore not possible to estimate the anisotropy using  $V_s$  with the 35 cm × 35 cm × 14 cm blocks.

Another objective of the preliminary tests was to perform US and IMA tests on a small number of specimens covering a wide temperature range. The tests were carried out on 5 cm × 5 cm × 30 cm prismatic specimens, one at 20 °C and one every 100 °C from 200 °C to 800 °C. From visual observations, as temperature ranged from 20 °C to 500 °C, a colour gradient appeared from beige (natural colour of the stone) to red (Fig. 2) due to the rubefaction of the limestone [7]. As soon as 800 °C was reached, the surface of the samples became white, showing that the decarbonation process had started. The sample crumbled easily and it could be considered that the material no longer had any mechanical strength. This colour gradient has also been found in the thickness of the vaults of the NDP cathedral [9].

The elastic modulus and Poisson's ratio values obtained on the 5 cm × 5 cm × 30 cm prisms are presented in Fig. 3. The values of  $E_{IMA}$  are higher than  $E_{US}$  by about 14% at 20 °C. The value of 13.4 GPa

**Fig. 2** Colour gradient of limestone 5 × 5 × 30 samples heated up to 800 °C



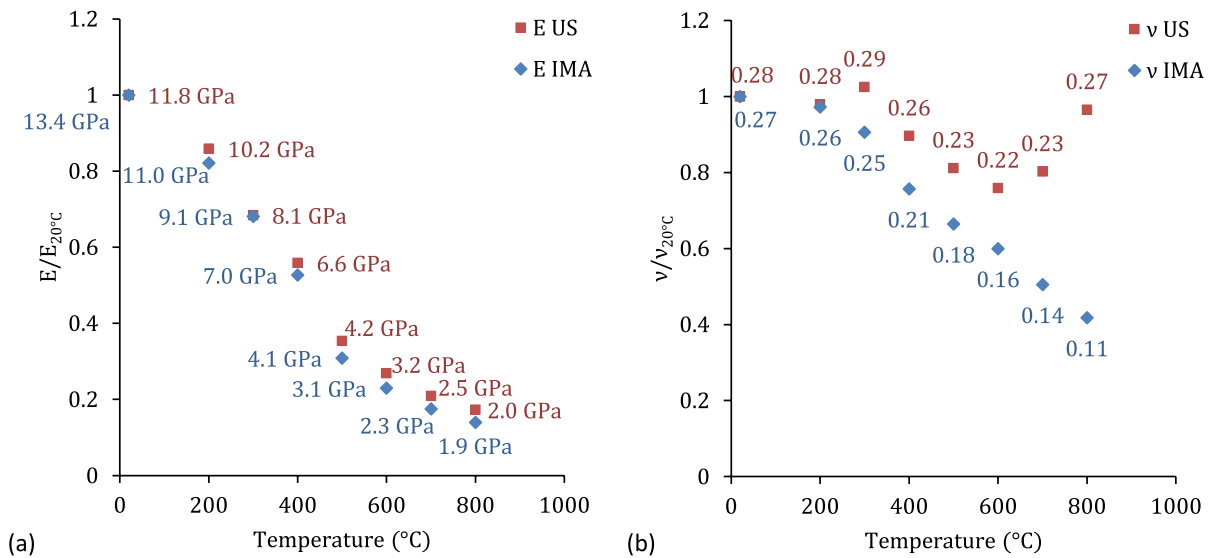


**Fig. 3** Moduli of elasticity **a** and Poisson's ratios **b** obtained by US and IMA

for  $E_{\text{IMA}}$  is very close to the  $E_{\text{stat}}$  obtained by Vigroux [6], i.e. 13.6 GPa, while the  $E_{\text{US}}$  measured here is equal to the  $E_{\text{US}}$  measured by Vigroux, i.e. 11.8 GPa. It can be seen that the evolution of these two values with temperature is remarkably similar, with a decrease of 32% at 300  $^\circ\text{C}$  and 75% at 600  $^\circ\text{C}$ . As for the Poisson's ratio, both measurements agree at 20  $^\circ\text{C}$  with Vigroux's  $v_{\text{stat}}$  value of 0.27, but diverge rapidly with temperature:  $v_{\text{IMA}}$  shows a linear decrease from 200  $^\circ\text{C}$  onwards while  $v_{\text{US}}$  describes a less predictable trajectory.

In light of these preliminary results, it was possible to select three temperatures of interest for the main experimental campaign. The first temperature chosen was 20  $^\circ\text{C}$ . The two additional temperatures should reflect the beginning and end of the thermal damage of the material. A first temperature of 300  $^\circ\text{C}$  was selected, where a decrease in the modulus of elasticity has already been observed, but where the compressive strength is not yet impacted according to Vigroux [6]. The second temperature chosen was 600  $^\circ\text{C}$ , which corresponds to a material very damaged in terms of both rigidity and strength.

## 4 Results

For each of the temperatures selected above, nine 7 cm  $\times$  14 cm cylindrical specimens and nine

5 cm  $\times$  5 cm  $\times$  30 cm prismatic specimens were tested by means of US and IMA methods. Among these specimens, six cylindrical samples were then tested in compressive tests and six prisms in 3PB tests. Finally, the two ends resulting from the 3PB tests were used for compressive tests and thermal tests.

### 4.1 Ultrasonic testing

Values of  $V_s$  and  $V_p$  were measured on the 7 cm  $\times$  14 cm cylindrical and 5 cm  $\times$  5 cm  $\times$  30 cm prismatic samples. The graphs in Fig. 4 show the results obtained on these samples before heating and after heating and cooling. A trend curve relating the density to the speed of the US waves is proposed, without distinction of sample geometry. There is little variability in density, the CV being only 2% for an average of 1754 kg/m<sup>3</sup>. Furthermore, the evolution of density with temperature is very small (3% mass loss after heating to 600  $^\circ\text{C}$ ). On average over all the samples,  $V_{p,20^\circ\text{C}}$  was measured at 2842 m/s and  $V_{s,20^\circ\text{C}}$  at 1557 m/s, with CVs of 2% for the prisms and 4% for the cylinders. The  $V_p$  falls within 5% of the value given by Vigroux at 297 m/s. The velocities  $V_p$  and  $V_s$  decrease by 11% and 10% respectively at 300  $^\circ\text{C}$ , and by 46% and 45% at 600  $^\circ\text{C}$ .

However, differences exist depending on the geometry of the sample. On average at 20  $^\circ\text{C}$ , prisms show higher  $V_p$  than cylinders, with deviations of +2.3%





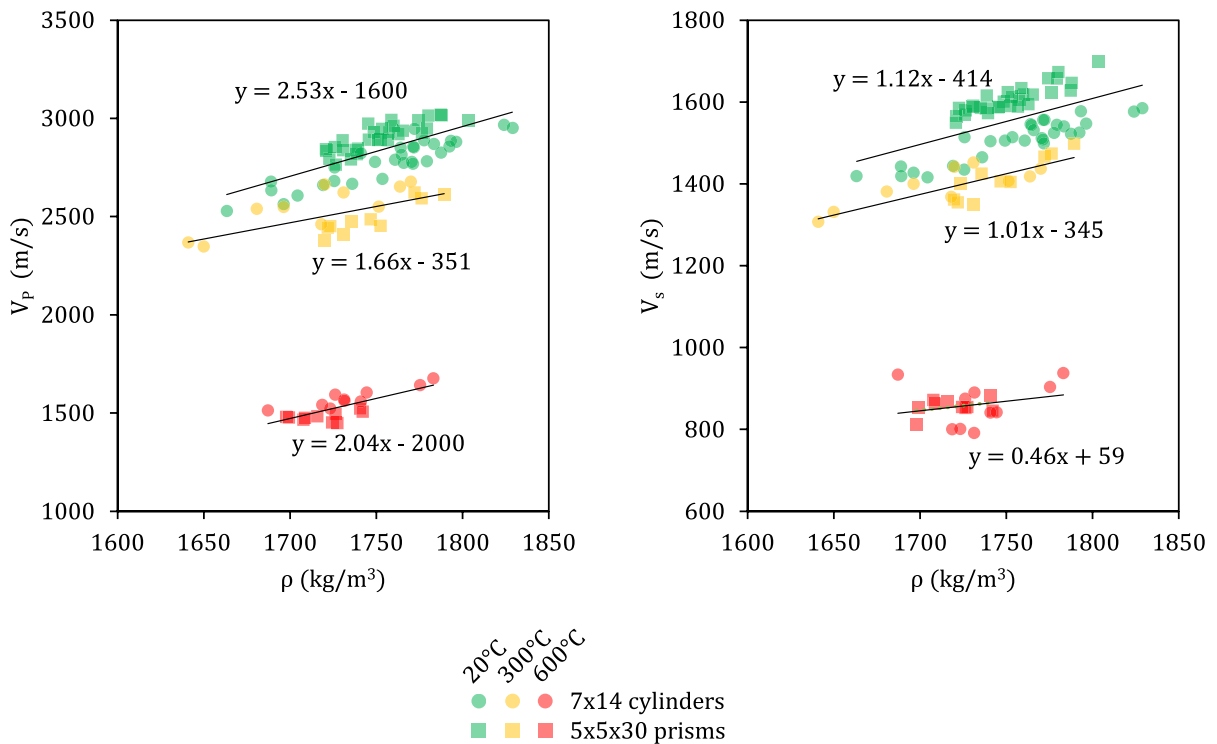


**Fig. 4** Effect of temperature on US velocities  $V_p$  and  $V_s$

and  $-2.4\%$  respectively from the trend curve. This difference is reversed for heated samples, with the cylinders showing higher  $V_p$  than the prisms, with deviations of  $+2.2\%$  and  $-2.2\%$  respectively from the trend curve. These deviations are more pronounced for the  $V_s$  measurements at  $20^\circ\text{C}$ :  $+3.2\%$  for the prisms and  $-3.5\%$  for the cylinders. There is no significant deviation related to the geometry in  $V_s$  measurements ( $<0.5\%$ ) for heated samples. These observations show that the prisms undergo greater degradation of  $V_p$  and  $V_s$  than the cylinders.

Using Eqs. 1 and 2, the values of the dynamic modulus of elasticity and Poisson's ratio can be derived from  $V_p$  and  $V_s$ . The results are plotted in Fig. 5 along with IMA values that will be discussed later. On average at  $20^\circ\text{C}$ ,  $E_{us}$  is estimated to be  $11.7\text{ GPa}$  for prisms and  $10.3\text{ GPa}$  for cylinders, while the  $\nu_{us}$  is estimated to be  $0.28$  for prisms and  $0.29$  for cylinders. The difference of US velocities between geometries is therefore initially small, about  $5\%$  to  $6\%$ , but produces a difference of more than  $13\%$  on the calculation of the dynamic Young's modulus. On average over the two geometries, the modulus is

$11.0\text{ GPa}$  and the Poisson's ratio is  $0.29$  at  $20^\circ\text{C}$ . This is consistent with  $E_{us} = 11.8\text{ GPa}$  obtained by Vigroux on  $4\text{ cm} \times 8\text{ cm}$  cylindrical samples. Then, at  $300^\circ\text{C}$ , the average modulus decreases by  $21\%$  and the Poisson's ratio by  $4\%$ . At  $600^\circ\text{C}$ , these same properties decrease by a total of  $71\%$  and  $6\%$  respectively. The small change and the rather high variability in  $\nu_{us}$  measurements tend to validate the previous statement about their unpredictability (Fig. 3).

#### 4.2 IMA testing

The values of  $E_{IMA}$  and  $\nu_{IMA}$  are presented in Fig. 5 against  $E_{us}$  and  $\nu_{us}$ . There is a good correlation between  $E_{IMA}$  and  $E_{us}$ , but this is not the case however for the  $\nu$  results. The IMA results seem to reflect the evolution of Poisson's ratio with temperature much better than the US results, although there is a higher data dispersion. On average over all the samples at  $20^\circ\text{C}$ , the  $E_{IMA}$  is  $12.8\text{ MPa}$  and the  $\nu_{IMA}$  is  $0.24$ . With heating, these properties decrease to  $10.0\text{ MPa}$  and  $0.23$  respectively at  $300^\circ\text{C}$ , then to  $3.7\text{ MPa}$  and  $0.16$  at  $600^\circ\text{C}$ . These values must be

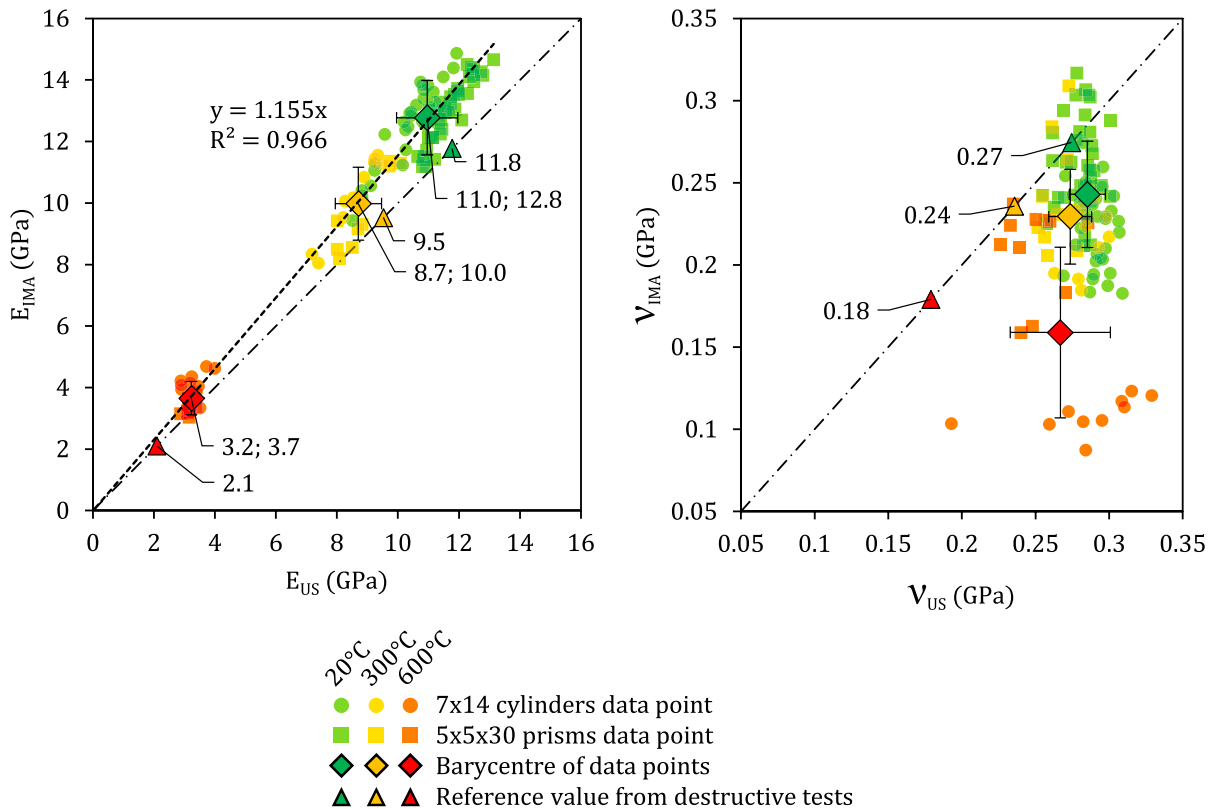


**Fig. 5** Effect of temperature on non-destructive measurements of Young modulus (left) and Poisson's ratio (right)

put into perspective with regard to their CV: elasticity modulus varies between 4 and 9% of the mean value, and that is mainly linked with density variation. In contrast, Poisson's ratio shows a CV between 12 and 21%, without correlation to density.

Concerning the differences between sample geometries, the  $E_{IMA}$  shows the same pattern as described above with  $E_{US}$  measurements: the modulus measured at 20 °C on prisms is, on average, 4% higher than that measured on cylinders but, at 300 °C and 600 °C, it shows greater degradation and is 5% and 22% lower.

#### 4.3 Compressive and 3PB testing

Consecutively to the US and IMA testing, six cylindrical samples were subjected to uniaxial compressive tests and six prismatic samples to 3PB tests. The results are shown in Fig. 6. At 20 °C on average,  $E_{stat}$  is 11.8 GPa, and  $\sigma_t$  is 2.4 MPa. The average  $\epsilon_{c,peak}$  is  $1.27 \cdot 10^{-3}$ , and the  $\nu_{stat}$  is measured at 0.27. With temperature,  $E_{stat}$  and  $\sigma_t$  decrease similarly,

by about 20% at 300 °C and 75% at 600 °C, while  $\epsilon_{c,peak}$  increases by 23% at 300 °C and by 213% at 600 °C. Finally, Poisson's ratio decreases by 14% and 35% at 300 °C and 600 °C. The CVs found on these measurements generally vary from 5 to 15%, with the greatest dispersion, of 21%, being observed on  $\nu_{stat}$  at 300 °C.

Furthermore, samples of other geometries were tested in compression, such as 10 cm × 10 cm × 10 cm cubes (three per temperature) and 5 cm × 5 cm × 5 cm cubes (ten per temperature). The comparative results in  $\sigma_c$  are plotted in Fig. 7. A 70% confidence interval is proposed based on results at 20 °C, 300 °C and 600 °C. The average  $\sigma_{c,10}$  at 20 °C, which corresponds to the standard reference strength, is 11.0 MPa. The  $\sigma_{c,7}$  at 20°C is 11.5 MPa, and  $\sigma_{c,5}$  is 11.9 MPa. The strength is constant up to around 300 °C, or even increases slightly. Then, at 600 °C, the strength is significantly reduced to between 60 and 80% of its initial value. The differences observed between the geometries, both at ambient temperature and with heated



**Fig. 6** evolution with temperature of mechanical properties measured during compressive tests on  $7 \times 14$  samples and bending tests on  $5 \times 5 \times 30$  samples

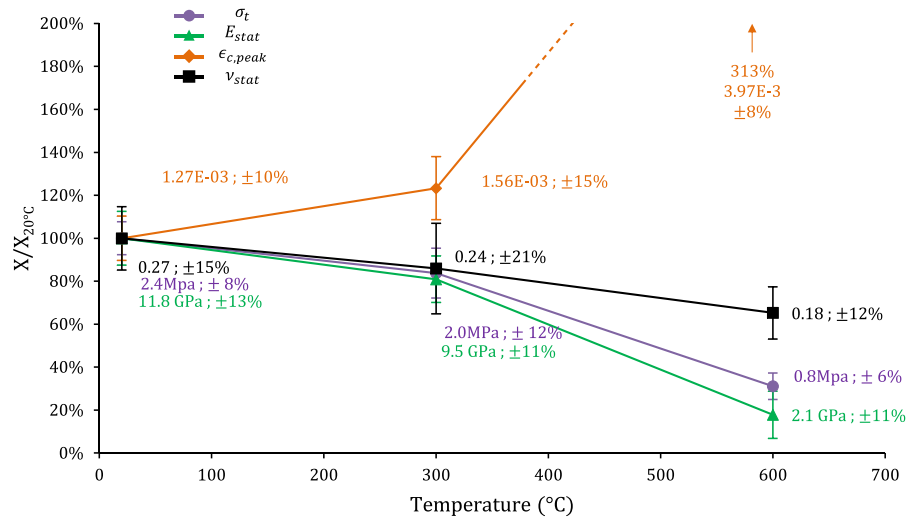
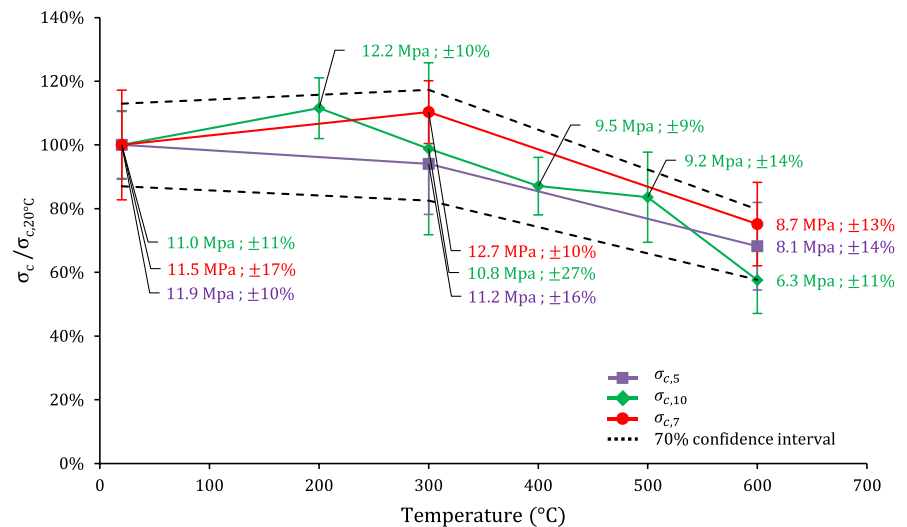


**Fig. 7** Compressive strength of samples  $5 \times 5 \times 5$  ( $\sigma_{c,5}$ ),  $10 \times 10 \times 10$  ( $\sigma_{c,10}$ ),  $7 \times 14$  ( $\sigma_{c,7}$ ), as a function of temperature



samples, are not significant with respect to the rather high variability ranging from 10 to 27%.

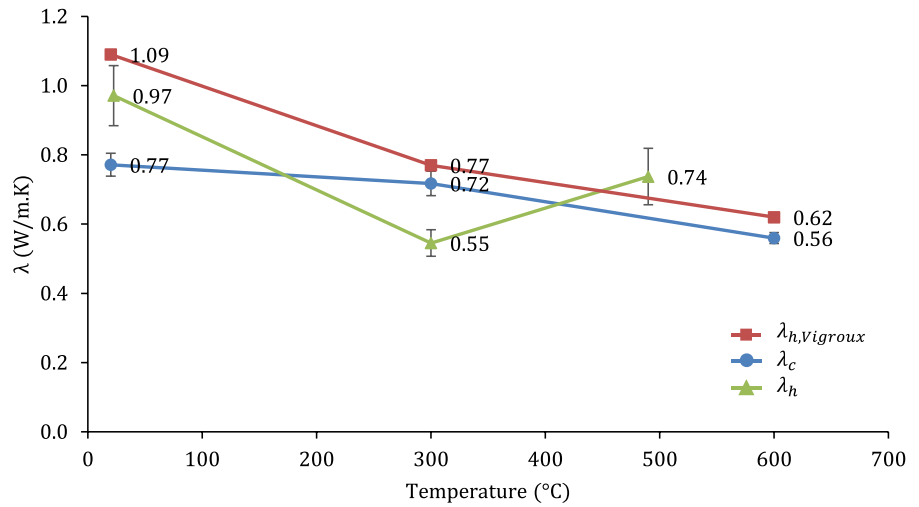
#### 4.4 Thermal testing

The purpose of thermal characterization is to determine the thermal characteristics during heating and after cooling necessary to run a thermo-mechanic simulation (thermal conductivity, heat capacity and density). Density has already been measured in the previous parts. Thermal conductivity was measured on hot material ( $\lambda_h$ ) and cooled material ( $\lambda_c$ ) using XFA/DSC measurements and hot wire measurements, respectively. The results are shown in Fig. 8,

together with results obtained by Vigroux with the hot disk method ( $\lambda_{h,Vigroux}$ ). The hot wire method yielded  $\lambda_c$  results with low variation (CV < 5% over nine samples). The DSC measurements of  $C_{p,h}$  (CV < 2% over 15 values) and XFA measurements of  $a_h$  (CV between 5 and 8% over 30 values) give an estimation of  $\lambda_h$  with a maximum uncertainty of 12%. At 20 °C, the XFA/DSC method gave  $\lambda_h = 0.97$  W/m K and the hot wire method gave  $\lambda_c = 0.77$  W/m K. At this temperature, the results obtained by Vigroux using the hot disk method are quite different from those measured with the hot wire. However, when results for hot samples at 300 °C and 600 °C ( $\lambda_{h,Vigroux}$ ) were compared



**Fig. 8** Measurements of thermal conductivities obtained on hot samples (XFA/DSC method) and cold samples (hot wire method)



with those of cooled samples ( $\lambda_c$ ), they proved to be close. The possible presence of moisture in Vigroux's samples could explain the higher conductivity at ambient temperature, as the materials in the present study were verified to be dry. On the other hand,  $\lambda_h$  showed a minimum of 0.55 at 300 °C before rising to 0.74 W/m K at 500 °C, a behaviour very different from that observed previously.

The intermediate results of the XFA/DSC method, i.e.  $C_{p,DSC}$  and  $a_{XFA}$ , are presented in Fig. 9 together with  $C_{p,calo}$  results. The  $a_h$  decreases from 7.0 J/kg K to 2.5 J/kg K between 20 °C and 480 °C. Over the same temperature range,  $C_{p,h}$  increases from 0.78 cm<sup>2</sup>/s to 1.73 cm<sup>2</sup>/s. Although the  $a_h$  measurements are consistent with that made by Vigroux, the  $C_{p,h}$  measured with DSC shows a significant slope

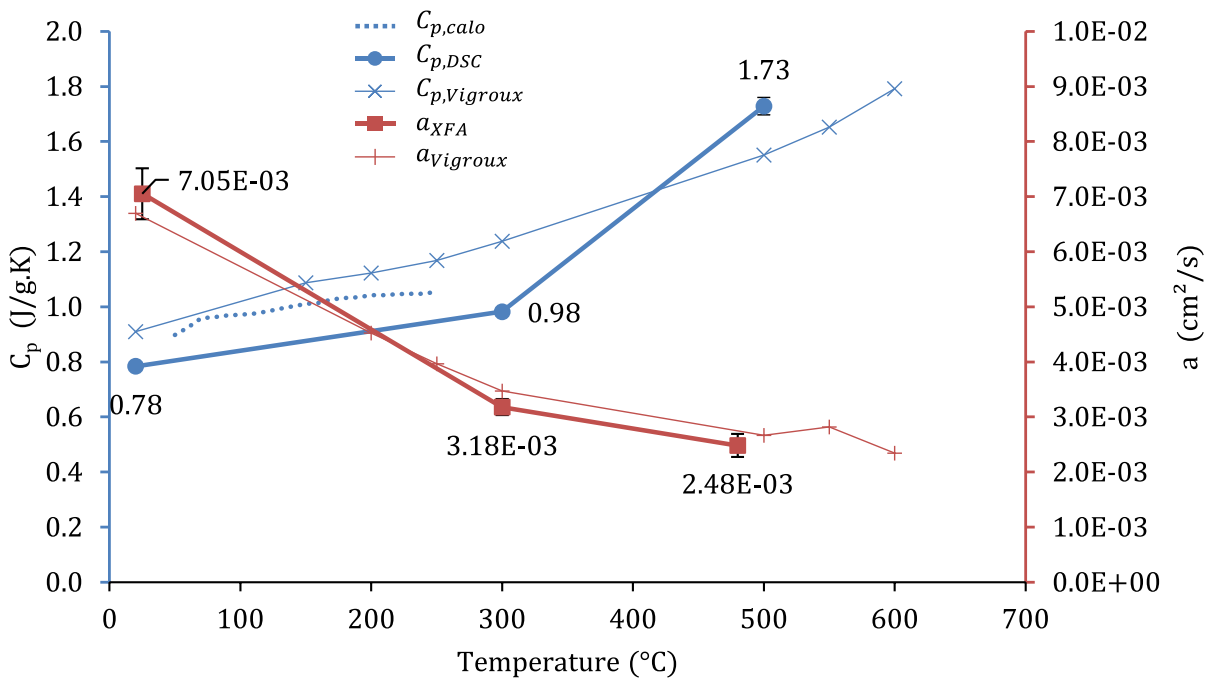


**Fig. 9** Measurement of intermediate thermal properties of hot stone



increase between 300 °C and 500 °C, which causes the increase of  $\lambda_h$  between 300 °C and 500 °C noted above. The  $C_{p,calo}$  measurements show how keeping the microstructure affects the heat capacity: when the material was not ground, the measurements were much closer to those Vigroux found with the hot disk. Unfortunately, the equipment could not heat the sample above 300 °C to compare with the rest of the data.

## 5 Discussion

The results presented in the previous section concern a range of samples of different geometries and sizes that were subjected to both destructive and non-destructive mechanical testing, as well as thermal testing. It allows results obtained in different ways to be compared and cross-checked. In addition, the heating of these samples allows the discussion to be widened by introducing the effect of temperature on the mechanical properties of the stone. The results discussed here were obtained after cooling of the samples.




### 5.1 Mechanical characterization

Two non-destructive methods, US and IMA, were implemented in this study to measure both elastic characteristics  $E$  and  $\nu$ . As stated before, the size and the shape of the sample are important parameters of the US testing method and can explain most of the 13% difference on  $E_{us}$  observed at 20 °C between 5 cm × 5 cm × 30 cm and 7 cm × 14 cm samples. In contrast, the measurements made using IMA showed

little difference between geometries at 20 °C with regard to the CV. Compressive tests gave very reliable data showing a linear decrease of  $\nu$  with increasing temperature, which was detected with IMA but not with US. However, for Young's modulus, US, IMA and compressive tests gave close results of at 20 °C and at high temperatures. There is a good correlation between  $E_{IMA}$  and  $E_{US}$ , and both the US and IMA methods give very acceptable lower and upper limits for estimating Young's modulus between 20 °C and 300 °C. These elements confirm the advantages of the IMA method for estimating the elastic mechanical properties of heated and cooled stone samples.

Shape and scale effects are important phenomena commonly observed in rocks and are taken into account in standard EN 772-1 [22] through shape factors to be applied to the compressive strength measured with reference to  $\sigma_{c,10}$ . These coefficients express the decrease in compressive strength as the volume of the sample and the slenderness increase. Shape factors for Saint-Maximin stone calculated from the experimental results of the present study are presented in Table 2, in the aim of evaluating whether the heating of the stones modifies the shape coefficients. The standard shape factors are also shown for comparison. With an average standard deviation around 15% for the compressive strength measurements over all the different temperatures tested, a deviation of less than 30% for the stress ratios is not significant. This is the case for all the samples at room temperature, which means that the tests on Saint-Maximin stone do not reveal any volume or slenderness effect. This observation is consistent with previous work that has shown that the scale effect is small in soft rock, as

**Table 2** Comparative table of shape factors by temperature

		$\sigma_{c,10}$ 	$\sigma_{c,5}$ 	$\sigma_{c,7}$ 
Shape		10 × 10 × 10	5 × 5 × 5	7 × 14
Volume (cm <sup>3</sup> )		1000	125	539
Slenderness ratio		1	1	2
Compressive strength (MPa) ± SD % (number of samples)	At 20 °C	11.0 ± 11% (3)	11.9 ± 10% (13)	11.5 ± 17% (6)
	At 300 °C	10.8 ± 27% (3)	11.2 ± 16% (10)	12.7 ± 10% (6)
	At 600 °C	6.3 ± 11% (3)	8.1 ± 14% (10)	8.7 ± 13% (6)
Shape factor	At 20 °C (EN 772-1)	1.0	0.85	1.24
	At 20 °C (present study)	1.0	0.92	0.96
	At 300 °C	1.0	0.96	0.85
	At 600 °C	1.0	0.77	0.72

opposed to hard rock [25], and that there is little or no slenderness effect in limestone for L/D ratios below 2 [26]. It is shown here that this soft limestone does not exhibit any of the behaviours described in the EN 772–1 Standard with regard to slenderness and volume effects. As a matter of fact, the EN 772–1 Standard applies for all masonry units outlined in EN 1996 (Eurocode 6), which includes, in addition to natural stone, clay, calcium silicate, aggregate concrete, autoclaved aerated concrete and manufactured stone units. Such a diversity of masonry units, not even considering the diversity within each unit category, implies a diversity of mechanical behaviour that cannot be represented by a single shape factor. The same observation can be made up to 300 °C. However, at 600 °C, there is a significant decrease in the aspect ratio. As the 5 cm×5 cm×5 cm and 7 cm×14 cm samples show a similar decrease, it can be concluded that slenderness is not responsible and that the volume effect is the main reason for this decrease at 600 °C.

Using Eqs. 11 and 12 from [4], it is possible to compare our data with regard to correlation equations previously established on a large population of samples representing limestones from around the world (Fig. 10). A 90% confidence interval is plotted, based on all the experimental results gathered together in [4]. Data points extracted from the same study but corresponding specifically to Lutetian limestone are also plotted. Saint-Maximin limestone is one of the softer limestones and is therefore among the lowest values reported. It can be seen that both correlations remain valid at 20 °C and 300 °C, inside the confidence interval and well within the Lutetian limestone points. However, the

points of the samples heated to 600 °C are outside the confidence intervals, showing that the correlations are not valid at this temperature.

$$\sigma_c = 2.65 \cdot 10^{-9} \times V_p^{2.75} \quad (11)$$

$$\rho = 946 \ln(V_p) - 5561 \quad (12)$$

## 5.2 Thermal characterization

Two methods were implemented in order to measure heat conductivity on hot and on cooled samples, and their results were compared with those on hot samples from a previous study. Considering that the possible moisture difference of the samples explains the discrepancy at 20 °C, the results of hot disk (on hot material) and hot wire (on cooled samples) agree that the cooling process induces only a 0.06 W/m K decrease in thermal conductivity of Saint-Maximin stone. The close similarity between  $a_h$  and the diffusivity obtained by Vigroux is valuable information, proving the thermal similarity between the ‘franche fine’ and ‘ferme fine’ Saint-Maximin stone.

Additionally, the conditioning of the material (ground or not) induces a change in the thermal behaviour of the material that is observed in  $C_p$  measurements. Reducing the sample to powder changes the microstructure and porosity of the stone, which alters the heat transfer characteristics. Direct comparisons between powdered and intact samples are therefore unreliable.

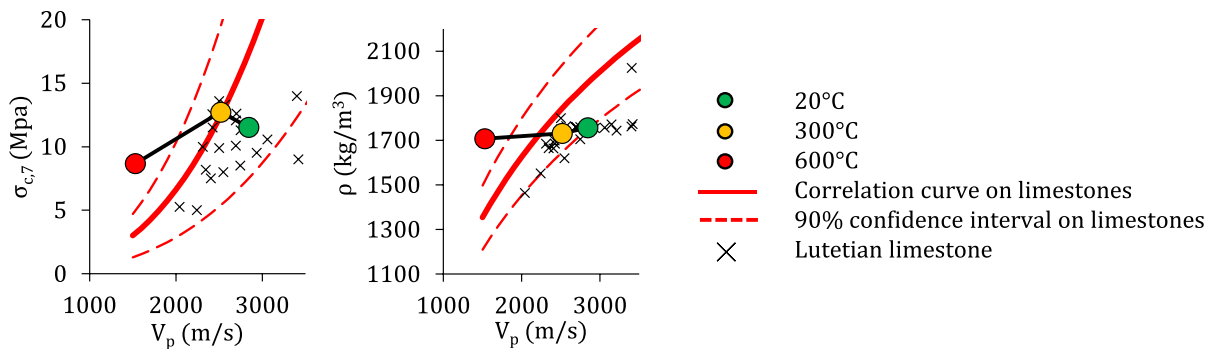


**Fig. 10** Display of the Saint-Maximin stone data in relation to the Lutetian limestone specifically and to the correlation formula for limestones proposed by [4]



## 6 Conclusion

In order to analyse the post-fire mechanical behaviour of NDP cathedral, an extensive experimental campaign, both destructive and non-destructive, was carried out on a Lutetian limestone similar to that identified in the vaults of the NDP cathedral, the Saint-Maximin stone. This campaign is intended to provide the elements necessary to feed the material parameters of a numerical model from a mechanical and thermal point of view, considering the effect on these properties of temperatures up to 800 °C.

According to the ultrasonic velocities obtained, the material can be considered isotropic. The increase of the temperature decreases the static modulus of elasticity and the Poisson's ratio.

Non-destructive testing has shown that the usual correlation equations linking US measurements and mechanical properties are not valid for stone samples that have been heated. This is particularly the case for the estimation of the Poisson's ratio. As this study was carried out only on Saint-Maximin stone, a very porous Lutetian limestone, stones of different lithologies should also be studied to see if this conclusion remains valid. In addition, the US measurement method has shown a geometry bias for samples with small cross-sections. However, an alternative measurement method by IMA is proposed which gives results very close to those obtained by destructive testing. Further research is required to apply this method to cylinders sampled from fire-damaged structures, as such samples are likely to exhibit a temperature gradient along their length. Also, an alternative method for performing IMA measurements using a microphone instead of an accelerometer could be developed in the future to assess the elastic mechanical properties on hot materials.

Uniaxial compression tests on specimens of different sizes and geometries also made it possible to estimate shape factors specific to Saint-Maximin stone. They are in contradiction with those proposed in the current European Standards for stone, since there is little to no scale effect or slenderness effect on Saint-Maximin stone. However, a scale effect does appear after the rock has been heated to 600 °C. New shape factors were then proposed at 600 °C to account for this geometry effect on the compressive strength. The proposed shape factors deserve to be confirmed by an experimental campaign on a larger number

of samples, given the large scatter of experimental results. Finally, the results obtained showed that the various correlations established for stones (or at least for Lutetian limestones) remain valid at 20 °C, but this is not necessarily the case when the samples are heated. It stays acceptable up to 300 °C because the structural thermal damage is low, but this is no longer the case at 600 °C. From the comparison with another limestone, these results suggest that the effects of temperature on elastic modulus damage and on compressive strength damage are phenomenologically different.

**Acknowledgements** The authors express their gratitude to the French National Research Agency (ANR) for supporting their investigations, and to Rocamat for providing the stone samples. The authors thank *Susan Becker* for her help in proofreading.

**Author contribution** All authors contributed to the conception and design of the study. Resources and equipment were provided by S. Corn and M. Salgues. Material preparation, data collection, analysis and writing of the first draft were carried out by C. Guenser. The manuscript was discussed and revised by all authors. All authors read and approved the final version of the manuscript. The study was supervised by N. Domede.

**Funding** Agence Nationale de la Recherche (ANR-20-CE22-0004).

### Declarations

**Conflict of interest** The investigations and results reported here were supported by the French National Research Agency (ANR) under the grant ANR-20-CE22-0004 (DEMMEFI research program). The authors have no competing interests to declare that are relevant to the content of this article.

## References

1. Deldicque DS, Rouzaud J-N (2020) Températures atteintes par la charpente de Notre-Dame de Paris lors de l'incendie du 15 avril 2019 déterminées par la paléothermométrie Raman. *C R Géosci* 352:7–18. <https://doi.org/10.5802/crgeos.9>
2. Praticò Y, Ochsendorf J, Holzer S, Flatt RJ (2020) Post-fire restoration of historic buildings and implications for Notre-Dame de Paris. *Nat Mater* 19:817–820. <https://doi.org/10.1038/s41563-020-0748-y>
3. Sciarretta F, Eslami J, Beaucour A-L, Noumowé A (2021) State-of-the-art of construction stones for masonry exposed to high temperatures. *Constr Build Mater* 304:124536. <https://doi.org/10.1016/j.conbuildmat.2021.124536>
4. Parent T, Domede N, Sellier A, Mouatt L (2015) Mechanical characterization of limestone from sound velocity



- measurement. *Int J Rock Mech Min Sci* 79:149–156. <https://doi.org/10.1016/j.ijrmmms.2015.08.009>
5. Brotons V, Tomás R, Ivorra S et al (2016) Improved correlation between the static and dynamic elastic modulus of different types of rocks. *Mater Struct* 49:3021–3037. <https://doi.org/10.1617/s11527-015-0702-7>
  6. Vigroux M, Eslami J, Beaucour A-L et al (2021) High temperature behaviour of various natural building stones. *Constr Build Mater* 272:121629. <https://doi.org/10.1016/j.conbuildmat.2020.121629>
  7. Vigroux M, Sciarretta F, Eslami J et al (2022) High temperature effects on the properties of limestones: post-fire diagnostics and material's durability. *Mater Struct* 55:253. <https://doi.org/10.1617/s11527-022-02086-5>
  8. Hawkins AB (1998) Aspects of rock strength. *Bull Eng Geol Environ* 57:17–30. <https://doi.org/10.1007/s100640050017>
  9. Dabat T, Mertz J-D, Leroux L, Meline Y (2021) Cathédrale Notre-Dame de Paris : Voûtes effondrées, murs bahuts et pignons, Caractérisation des carottes de pierre prélevées après l'incendie du 15 avril 2019. Laboratoire de recherche des monuments historiques, Champs-sur-Marne, France
  10. AFNOR (1999) EN ISO 834-1—Fire-resistance tests—elements of building construction—part 1: general requirements. AFNOR, La Plaine Saint-Denis France
  11. Binda L, Saisi A, Tiraboschi C (2001) Application of sonic tests to the diagnosis of damaged and repaired structures. *NDT E Int* 34:123–138. [https://doi.org/10.1016/S0963-8695\(00\)00037-2](https://doi.org/10.1016/S0963-8695(00)00037-2)
  12. Domede N, Parent T, Guenser C et al (2024) Mechanical characterization of the stones of Notre-Dame de Paris by in situ sonic auscultation. *Int J Rock Mech Min Sci* 175:105671. <https://doi.org/10.1016/j.ijrmmms.2024.105671>
  13. AFNOR (2004) Natural stone test methods—determination of sound speed propagation. AFNOR, La Plaine Saint-Denis France
  14. Cuxac P (1991) Propagation et atténuation des ondes ultrasoniques dans des roches fissurées et anisotropes. Institut National Polytechnique de Lorraine, Nancy
  15. PROCEQ (2013) PUNDIT PL-200 operating instructions. PROCEQ, Schwerzenbach
  16. Guyader J, Denis A (1986) Propagation des ondes dans les roches anisotropes sous contrainte. Évaluation de la qualité des schistes ardoisiers. *Bull Int Assoc Eng Geol* 33:49–55. <https://doi.org/10.1007/BF02594705>
  17. Fort R, Varas MJ, Alvarez de Buergo M, Martin-Freire D (2011) Determination of anisotropy to enhance the durability of natural stone. *J Geophys Eng* 8:S132–S144. <https://doi.org/10.1088/1742-2132/8/3/S13>
  18. Christaras B, Auger F, Mosse E (1994) Determination of the moduli of elasticity of rocks. Comparison of the ultrasonic velocity and mechanical resonance frequency methods with direct static methods. *Mater Struct* 27:222–228. <https://doi.org/10.1007/BF02473036>
  19. Saad A, Bost M (2009) The resonant frequency measurement and cracking evolution in rocks. ISRM, Dubrovnik-Cavtat
  20. Fogue-Djombou YI, Corn S, Clerc L et al (2019) Freezethaw resistance of limestone roofing tiles assessed through impulse vibration monitoring and finite element modeling in relation to their microstructure. *Constr Build Mater* 205:656–667. <https://doi.org/10.1016/j.conbuildmat.2019.01.211>
  21. AFNOR (2007) Natural stone test methods—determination of flexural strength under concentrated load. AFNOR, La Plaine Saint-Denis France
  22. AFNOR (2015) Methods of test for masonry units—part 1: determination of compressive strength. AFNOR, La Plaine Saint-Denis France
  23. Gustafsson SE (1991) Transient plane source techniques for thermal conductivity and thermal diffusivity measurements of solid materials. *Rev Sci Instrum* 62:797–804. <https://doi.org/10.1063/1.1142087>
  24. Chi W, Sampath S, Wang H (2006) Ambient and high-temperature thermal conductivity of thermal sprayed coatings. *J Therm Spray Technol* 15:773–778. <https://doi.org/10.1361/105996306X146730>
  25. Yoshinaka R, Osada M, Park H et al (2008) Practical determination of mechanical design parameters of intact rock considering scale effect. *Eng Geol* 96:173–186. <https://doi.org/10.1016/j.enggeo.2007.10.008>
  26. Tuncay E, Hasancebi N (2009) The effect of length to diameter ratio of test specimens on the uniaxial compressive strength of rock. *Bull Eng Geol Environ* 68:491–497. <https://doi.org/10.1007/s10064-009-0227-9>

**Publisher's Note** Springer Nature remains neutral with regard to jurisdictional claims in published maps and institutional affiliations.

Springer Nature or its licensor (e.g. a society or other partner) holds exclusive rights to this article under a publishing agreement with the author(s) or other rightsholder(s); author self-archiving of the accepted manuscript version of this article is solely governed by the terms of such publishing agreement and applicable law.

